TIME REVERSAL IN CHANGING ENVIRONMENT

GUILLAUME BAL * AND RAMÓN VERÁSTEGUI †

Abstract. This paper analyzes the refocusing properties of time-reversed acoustic waves, which propagate in different media during the forward and backward propagation phases. We present the modifications of the refocused signal as the backward propagation medium departs from the forward propagation medium. The derivation is based on the analysis of the correlation of two fields propagating in different backgrounds. The correlation is described by the Wigner transform of the two fields, which satisfies in the limit of high frequencies a generalized radiative transfer equation. The theory is presented in two and three space dimensions in the transport and diffusive regimes. Numerical experiments show a remarkable agreement with theory.

Key words. Time reversal, waves in random media, radiative transfer regime, diffusion regime, Wigner transform, changing environment.

AMS subject classifications. 35R60 35L40 78A45 82D30

1. Introduction. Time reversed waves have striking refocusing property. A typical experiment is conducted as follows. A signal is emitted from a localized source and recorded by a detector array of small size. The recorded signal is then time-reversed and sent back into the *same* medium. When the underlying medium is heterogeneous, the back-propagated signal refocuses at the location of the original source much more tightly than when propagation occurs in a homogeneous medium. The reason is multipathing and is now quite well understood both physically and mathematically. We refer to [17, 18, 22, 23] for a presentation of the physical experiments, to [12, 21] for mathematical analyzes in one-dimensional or layered media, to [2, 5, 10, 25, 26] for three-dimensional waves in the parabolic regime, to [4, 6, 20] for analyzes of the three dimensional acoustic waves and to [8] for chaotic cavities. Time reversal has found many important applications, including biomedical engineering [19], imaging in cluttered environment [9, 11], and communication [14, 15].

Since multipathing and exact phase cancellations are crucial in ensuring the tight refocusing property of the time reversed waves, it is imperative that the back-propagated signal be emitted in the *same* heterogeneous medium as the forward propagating signal to obtain optimal refocusing. Even though the medium can be kept fixed in controlled experimental settings such as [20], this may not be the case in practical applications such as medical treatment [19] where the patient moves or such as underwater [15] or aerial communication [14] where both ends of the communication channel may move and the scattering properties of the channel may vary with time. Several studies have shown modifications of the refocused signal as the underlying medium changes [22, 29].

This paper presents an analysis of the refocusing modifications when the underlying media differ during the forward and the backward propagations. We assume that these media are fixed during both propagation phases. This framework models slow changes in the underlying medium compared to the propagation time. Applications include the slow drifting of the detectors before the signal is back-propagated or changes in the intensity of the background fluctuations that are responsible for the

*Department of Applied Physics and Applied Mathematics, Columbia University, New York NY, 10027; gb2030@columbia.edu

†Department of Applied Physics and Applied Mathematics, Columbia University, New York NY, 10027; rv2007@columbia.edu

enhanced refocusing properties of the time reversed waves. This is the setting of the experimental works in [22, 29] for instance. This is also the setting of the recent work [1] on a thorough analysis of time reversal in changing one-dimensional environment.

We consider acoustic waves propagating in two and three dimensional media with rapid and weak fluctuations. It is known that the wave energy density can then be modeled by radiative transfer equations in the high frequency limit [27, 28]. The underlying mathematical structure based on the analysis of two-point correlation functions using the Wigner transform has been first applied to the understanding of multi-dimensional time reversed waves in [10], where waves are modeled by a parabolic approximation. The full acoustic wave equations were then considered in the same regime in [6]. The latter reference is the starting point of our analysis. The main novelty of the present paper is that we need consider the two-point correlation of two fields propagating in two *different* media. The equations of radiative transfer are consequently modified to account for the two propagation backgrounds.

It is shown in [6] that the whole time reversal procedure may be interpreted as a filtering process, where each wavenumber of the original source term is multiplied by a certain value that depends on the geometry of the detector array and on the wave interactions with the underlying medium. We show that this picture remains valid though changes in the properties of the medium modify the filtering process. Expressions for the filter are given in the radiative transfer regime and in its diffusion approximation. We specifically analyze the modifications of the filter in the diffusive regime when the back-propagation medium is a shifted copy of the forward propagation medium, and when the former has fluctuations proportional to that of the latter. We finally present two-dimensional numerical simulations of acoustic wave propagation, which show a remarkable agreement with theory.

The rest of the paper is structured as follows. Section 2 presents the time reversal procedure and the results in [6] that lay at the core of our analysis. Our main assumptions on the underlying media and our main results on the modified filtering process in the radiative transfer regime are given in section 3. The filtering processes are further simplified in section 4 where the diffusive regime is considered. Less general than transport, the diffusive regime allows us to obtain very compact formulas (4.14) that emphasize how the signal is modified in changing environments. The generalized radiative transfer equations presented in section 3 are derived in section 5. Their derivation is quite technical and based on the machinery developed in [27]. To make them more accessible, we first derive the generalized radiative transfer equations in the simplified setting of a scalar equation of the Schrödinger type. We then briefly explain how the theory generalizes to the full wave equations. Finally section 6 is devoted to a numerical simulation of time reversal in changing environment. We solve the wave equation in a two-dimensional box with periodic boundary conditions. We underline the main effects on the refocusing in changing environment that arise in the diffusive regime treated in section 4.

2. Time Reversal in Radiative Transfer Regime. This section summarizes results obtained in [6] that describe the refocusing properties of time reversed high frequency waves propagating in weakly heterogeneous media.

2.1. Wave equation and hyperbolic system. We can model the propagation of acoustic waves in three-dimensional domains by the following wave equation for the pressure field $p(t,\mathbf{x})$:

$$\frac{1}{c^2(\mathbf{x})}\frac{\partial^2 p}{\partial t^2}(t,\mathbf{x}) = \Delta p(t,\mathbf{x}), \tag{2.1}$$

where $t > 0$ is time, $\mathbf{x} \in \mathbb{R}^3$ is position, $c(\mathbf{x})$ is the sound speed and Δ the usual Laplace operator. This equation is augmented with initial conditions, which we take of the form

$$p(0,\mathbf{x}) = p_0(\mathbf{x}), \qquad \frac{\partial p}{\partial t}(0,\mathbf{x}) = g(\mathbf{x}). \tag{2.2}$$

This is the equation that is discretized and solved numerically in section 6.

To perform the analysis of time reversal refocusing, it is more convenient to recast the wave equation as the following first-order hyperbolic system for the same pressure field $p(t,\mathbf{x})$ as above and the velocity field $\mathbf{v}(t,\mathbf{x})$:

$$\begin{aligned} &\rho\frac{\partial \mathbf{v}}{\partial t} + \nabla p = 0 \\ &\kappa(\mathbf{x})\frac{\partial p}{\partial t} + \nabla\cdot\mathbf{v} = 0, \end{aligned} \tag{2.3}$$

with initial conditions $p(0,\mathbf{x}) = p_0(\mathbf{x})$ and $\mathbf{v}(0,\mathbf{x}) = \nabla\varphi(\mathbf{x})$, where $\varphi(\mathbf{x})$ is obtained by solving

$$\Delta\varphi(\mathbf{x}) = \kappa(\mathbf{x})g(\mathbf{x}).$$

The density ρ is assumed to be constant to simplify and the compressibility $\kappa(\mathbf{x})$ is such that

$$\rho\kappa(\mathbf{x}) = \frac{1}{c^2(\mathbf{x})}.$$

Introducing the 4×4 matrix $A(\mathbf{x}) = \mathrm{Diag}(\rho,\rho,\rho,\kappa(\mathbf{x}))$, the 4×4 matrices $D^j_{mn} = \delta_{m4}\delta_{nj} + \delta_{n4}\delta_{mj}$, and the vector $\mathbf{u} = (\mathbf{v}, p)$, we recast (2.3) as

$$\begin{aligned} &A(\mathbf{x})\frac{\partial \mathbf{u}}{\partial t} + D^j\frac{\partial \mathbf{u}}{\partial x_j} = 0, \\ &\mathbf{u}(0,\mathbf{x}) = \mathbf{S}(\mathbf{x}), \end{aligned} \tag{2.4}$$

where $\mathbf{S}(\mathbf{x}) = (\nabla\varphi(\mathbf{x}), p_0(\mathbf{x}))$. We use the notation of summation over repeated indices so that the index j in the above equation is summed over $j \in \{1,2,3\}$.

2.2. Single-time time reversal framework. We consider the same time reversal framework as in [6]. It is described as follows. We first solve for $\mathbf{u}(t,\mathbf{x})$ in (2.4) on the time interval $(0,T)$. We denote by $\mathbf{u}(T^-,\mathbf{x})$ the solution at time T. We record that solution at an array of detectors defined by $\chi^2(\mathbf{x})$, where $\chi^2(\mathbf{x})$ is the amplitude of the detector at point $\mathbf{x}$ (thus $\chi^2(\mathbf{x}) = 0$ where there are no detectors). We then *time reverse* the solution and define

$$\mathbf{u}(T^+,\mathbf{x}) = \Gamma\chi^2(\mathbf{x})\mathbf{u}(T^-,\mathbf{x}),$$

where $\Gamma = \mathrm{Diag}(-1,-1,-1,1)$. This means that pressure is kept unchanged and that the velocity field is multiplied by -1. Next, the signal back-propagates in the same medium for the same duration T and is thus modeled by the following equation:

$$\begin{aligned} &A(\mathbf{x})\frac{\partial \mathbf{u}}{\partial t} + D^j\frac{\partial \mathbf{u}}{\partial x_j} = 0, \qquad T < t < 2T \\ &\mathbf{u}(T^+,\mathbf{x}) = \Gamma\chi^2(\mathbf{x})\mathbf{u}(T^-,\mathbf{x}). \end{aligned} \tag{2.5}$$

At time $2T$ we time reverse the signal a second time and define the back-propagated signal as

$$\mathbf{u}^B(\mathbf{x}) = \Gamma \mathbf{u}(2T, \mathbf{x}). \tag{2.6}$$

When $\chi^2(\mathbf{x}) \equiv 1$, i.e., when the whole signal is recorded at time $t = T^-$, we deduce from the *time reversibility* of the acoustics equations that $\mathbf{u}^B(\mathbf{x}) = \mathbf{S}(\mathbf{x})$. The striking result in time reversal is that in the case of limited data (typically, $\chi^2(\mathbf{x}) \neq 0$ only on a small domain in $\mathbb{R}^3$) $\mathbf{u}^B$ is much closer to the initial source term $\mathbf{S}(\mathbf{x})$ when propagation occurs in heterogeneous media than when it occurs in homogeneous media.

We call single-time time reversal the framework that analyzes the properties of the back-propagated signal $\mathbf{u}^B(\mathbf{x})$ originating from initial conditions $\mathbf{u}(0, \mathbf{x}) = \mathbf{S}(\mathbf{x})$. As was shown in [6], this framework is sufficient to understand the time reversal experiments in which the signal is recorded in time (and not at a single time) before time reversion as in [17, 23]. Indeed a signal recorded in time can be seen as a superposition of signals, each of which is analyzed in the single-time framework.

2.3. High frequency scaling. A macroscopic description of the back propagated signal $\mathbf{u}^B(\mathbf{x})$ can be obtained in the high frequency regime, where the width of the initial condition λ and the correlation length l of the underlying medium are small compared to the overall distances of propagation of size $L \sim c_0 T$, where c_0 is the average value of $c(\mathbf{x})$. We thus introduce the small parameter $\varepsilon = \lambda/L \ll 1$ and wish to understand $\mathbf{u}^B$ as $\varepsilon \to 0$. This is precisely the regime analyzed in [6]. The results of that theory are the following. We assume that the initial condition is of the form

$$\mathbf{u}(0, \mathbf{x}) = \mathbf{S}\Big(\frac{\mathbf{x} - \mathbf{x}_0}{\varepsilon}\Big) \tag{2.7}$$

and is thus centered around the point $\mathbf{x}_0$. Since we are interested in the refocused signal in the vicinity of $\mathbf{x}_0$, we introduce the scaling $\mathbf{x} = \mathbf{x}_0 + \varepsilon \boldsymbol{\xi}$ and the following notation for the back-propagated signal

$$\mathbf{u}^B(\boldsymbol{\xi}; \mathbf{x}_0) \tag{2.8}$$

to represent the back-propagated signal $\varepsilon\boldsymbol{\xi}$ away from the central point $\mathbf{x}_0$ of the initial source term. We assume that the compressibility has rapid but weak fluctuations

$$\kappa(\mathbf{x}) = \kappa_0 + \sqrt{\varepsilon}\kappa_1(\frac{\mathbf{x}}{\varepsilon}), \tag{2.9}$$

where κ_0 is a constant to simplify and κ_1 is a mean zero stationary random process with *two point correlation function* $R(\mathbf{x})$ defined by

$$\kappa_0^2 R(\mathbf{x}) = \langle \kappa_1(\mathbf{y})\kappa_1(\mathbf{y} + \mathbf{x})\rangle, \tag{2.10}$$

where $\langle \cdot \rangle$ denotes ensemble averaging over the realizations of the random media. We thus model our heterogeneous medium as one realization of a random process. We define the Fourier transform of a function $f(\mathbf{x})$ as

$$\hat{f}(\mathbf{k}) = \int_{\mathbb{R}^3} e^{-i\mathbf{k}\cdot\mathbf{x}} f(\mathbf{x}) d\mathbf{x}. \tag{2.11}$$

The *power spectrum* $\hat{R}(\mathbf{p})$ of the fluctuations $\kappa_1(\mathbf{x})$ is then defined as the Fourier transform of $R(\mathbf{x})$, and after some algebra it is shown to be such that

$$\langle \hat{\kappa}_1(\mathbf{p})\hat{\kappa}_1(\mathbf{q})\rangle = (2\pi)^3 \kappa_0^2 \hat{R}(\mathbf{p})\delta(\mathbf{p} + \mathbf{q}).$$

2.4. Macroscopic back-propagated signal. The main result obtained in [6, (3.31)] on the refocusing signal in the high frequency regime, i.e., in the limit $\varepsilon \to 0$, shows that

$$\hat{\mathbf{u}}^B(\mathbf{k};\mathbf{x}_0) = a_-(T,\mathbf{x}_0,\mathbf{k})\hat{\mathbf{S}}_+(\mathbf{k}) + a_+(T,\mathbf{x}_0,\mathbf{k})\hat{\mathbf{S}}_-(\mathbf{k}). \tag{2.12}$$

The notation is as follows. First, $\hat{\mathbf{u}}^B(\mathbf{k};\mathbf{x}_0)$ represents the Fourier transform of $\mathbf{u}^B(\boldsymbol{\xi};\mathbf{x}_0)$ in the first variable only. The source terms $\mathbf{S}_\pm$ are given in the Fourier domain by

$$\hat{\mathbf{S}}_\pm(\mathbf{k}) = \frac{\hat{p}_0(\mathbf{k})}{2}\left(\pm\sqrt{\frac{\kappa_0}{\rho}}\,\hat{\mathbf{k}}\,,\,1\right)^t + \frac{i|\mathbf{k}|\hat{\varphi}(\mathbf{k})}{2}\left(\hat{\mathbf{k}},\pm\sqrt{\frac{\rho}{\kappa_0}}\right)^t,$$

where $\hat{\mathbf{k}} = \mathbf{k}/|\mathbf{k}|$. We verify that the source term in (2.7) is such that $\mathbf{S} = \mathbf{S}_+ + \mathbf{S}_-$. The propagating modes $a_\pm$ measure the coherent interactions of the forward ($\mathbf{u}$ on $(0,T)$) and backward ($\mathbf{u}$ on $(T,2T)$) fields. They describe interactions propagating with velocity $\pm c_0$, respectively, where $c_0 = (\rho\kappa_0)^{-1/2}$. The corresponding vectorial source terms $\hat{\mathbf{S}}_\pm$ indicate how the velocity and pressure fields are coupled for each propagating mode. We refer to [6, 27] for additional details. The modes $a_\pm(t,\mathbf{x},\mathbf{p})$ solve the following radiative transfer equations:

$$\begin{aligned}&\frac{\partial a_\pm}{\partial t} \pm c_0\hat{\mathbf{k}}\cdot\nabla_{\mathbf{x}} a_\pm = \int_{\mathbb{R}^3}\sigma(\mathbf{k},\mathbf{p})(a_\pm(t,\mathbf{x},\mathbf{p}) - a_\pm(t,\mathbf{x},\mathbf{k}))\delta(c_0(|\mathbf{k}|-|\mathbf{p}|))d\mathbf{p}\\ &a_\pm(0,\mathbf{x},\mathbf{k}) = |\chi(\mathbf{x})|^2.\end{aligned} \tag{2.13}$$

The scattering coefficient $\sigma(\mathbf{k},\mathbf{p})$ is given by [27]

$$\sigma(\mathbf{k},\mathbf{p}) = \frac{\pi c_0^2}{2}|\mathbf{k}|^2\frac{\hat{R}(\mathbf{k}-\mathbf{p})}{(2\pi)^3} = \frac{c_0^2|\mathbf{k}|^2}{(4\pi)^2}\hat{R}(\mathbf{k}-\mathbf{p}). \tag{2.14}$$

Notice that $\hat{R}(\mathbf{p})$ is a non-negative function so that the transport equations (2.13) are well-posed [13]. To simplify we assume that the inhomogeneities are statistically isotropic so that $\hat{R}(\mathbf{p}) = \hat{R}(|\mathbf{p}|)$. The transport equations (2.13) can also be recast as

$$\begin{aligned}&\frac{\partial a_\pm}{\partial t} \pm c_0\hat{\mathbf{k}}\cdot\nabla_{\mathbf{x}} a_\pm + \Sigma a_\pm = \int_{\mathbb{R}^3}\sigma(\mathbf{k},\mathbf{p})a_\pm(t,\mathbf{x},\mathbf{p})\delta(c_0(|\mathbf{k}|-|\mathbf{p}|))d\mathbf{p}\\ &a_\pm(0,\mathbf{x},\mathbf{k}) = |\chi(\mathbf{x})|^2,\end{aligned} \tag{2.15}$$

where

$$\Sigma(|\mathbf{k}|) = \int_{\mathbb{R}^3}\sigma(\mathbf{k},\mathbf{p})\delta(c_0(|\mathbf{k}|-|\mathbf{p}|))d\mathbf{p} = \frac{c_0|\mathbf{k}|^4}{(4\pi)^2}\int_{S^2}\hat{R}(|\mathbf{k}||\hat{\mathbf{e}}-\hat{\mathbf{p}}|)d\hat{\mathbf{p}}, \tag{2.16}$$

with $\hat{\mathbf{e}}$ an arbitrary unit vector in S^2.

The interpretation of (2.12) is thus as follows. The time reversal experiment is modeled in the Fourier domain by a linear filtering. The filters are given by the solutions to the above radiative transfer equations. In the absence of randomness in the medium, $\sigma \equiv 0$ and the modes $a_\pm$ can be shown to be increasingly singular as T grows. We thus see that the shape of refocused signal is increasingly modified as T grows since $a_\pm$ goes further and further away from a constant value. In the presence of sufficient random scattering in the medium, the modes $a_\pm$ become instead increasingly regular thanks to the right-hand side in (2.13). This implies that the refocused signal

$\mathbf{u}^B$ will be much closer to the original source term $\mathbf{S}$ than when propagation occurs in homogeneous media; see [6] for the details.

Notice that $a_\pm(t,\mathbf{x},\mathbf{k})$ at different values of $|\mathbf{k}|$ satisfy decoupled equations. This is because scattering is elastic in this model so that the frequency $\omega = c_0|\mathbf{k}|$ is conserved in the scattering process.

3. Time Reversal in changing media. Let us now consider the case where the medium in which the signal is retransmitted is different from the medium in which it first propagates. In practice this corresponds to waiting for sufficiently long after recording the signal and before retransmitting it so that the underlying medium has changed slightly. We assume in this theory that the medium is stable during both the forward and the backward propagations. This assumption seems to cover many settings of practical interest, in which the time scales at which the media change are large compared to the propagation time T [17, 23].

3.1. Modeling of the changing environment. The main assumption in our model is that the medium in (2.5) during the back-propagation phase is now given by

$$\kappa_b(\mathbf{x}) = \kappa_0 + \sqrt{\varepsilon}\kappa_2(\mathbf{x}, \frac{\mathbf{x}}{\varepsilon}), \tag{3.1}$$

where the fluctuations κ_2 are of the form

$$\hat\kappa_2(\mathbf{x},\mathbf{k}) = \phi(\mathbf{x},\mathbf{k})\hat\kappa_1(\mathbf{k}), \tag{3.2}$$

Here $\hat\kappa_2$ denotes Fourier transform in the second variable only. The first variable $\mathbf{x}$ corresponds to changes in the fluctuations at the macroscopic scale. The second variable $\mathbf{k}$ corresponds to changes in the fluctuations at the microscopic scale. The function $\phi(\mathbf{x},\mathbf{k})$ models changes both in the global spatial (variable $\mathbf{x}$) and the local wavenumber (variable $\mathbf{k}$) domains. A function $\phi(\mathbf{x})$ indicates the factor by which the intensity of the random fluctuations has changed locally around $\mathbf{x}$ before retransmission. A function $\phi(\mathbf{k}) = e^{i\mathbf{k}\cdot\boldsymbol{\tau}}$ indicates a shift of the domain corresponding to

$$\kappa_2(\mathbf{x}) = \kappa_1(\mathbf{x}+\boldsymbol{\tau}).$$

Since $\kappa_{1,2}$ are real-valued functions, we impose that

$$\phi(\mathbf{x},-\mathbf{p}) = \phi^*(\mathbf{x},\mathbf{p}). \tag{3.3}$$

Here * denotes complex conjugation. We assume here that $\phi(\mathbf{x},\mathbf{k})$ is deterministic to simplify the presentation. Very similar results would also hold with κ_1 and κ_2 more general correlated random fields; see section 5.

3.2. Main result on back-propagated signal. The main result of this section is that the back-propagated signal still has the form given in (2.12). However the propagating modes now satisfy instead of (2.13) the following modified radiative transfer equations

$$\begin{aligned}&\frac{\partial a_\pm}{\partial t} \pm c_0\hat{\mathbf{k}}\cdot\nabla a_\pm + \Big(\sigma_a(\mathbf{k}) \pm i\Pi(\mathbf{k})\Big)a_\pm = Qa_\pm,\\ &a_\pm(0,\mathbf{x},\mathbf{k}) = |\chi(\mathbf{x})|^2.\end{aligned} \tag{3.4}$$

The terms and operators of the above equation are defined as follows:

$$\begin{aligned} Qa(\mathbf{k}) &= \int_{\mathbb{R}^3} \sigma(\mathbf{k},\mathbf{p})\phi(\mathbf{x},\mathbf{p}-\mathbf{k})\Big(a(\mathbf{p})-a(\mathbf{k})\Big)\delta(c_0(|\mathbf{k}|-|\mathbf{p}|))d\mathbf{p} \\ \Pi(\mathbf{k}) &= \fint_{\mathbb{R}^3} (1-|\phi(\mathbf{x},\mathbf{p}-\mathbf{k})|^2)\frac{c_0}{2}\frac{|\mathbf{k}||\mathbf{p}|^2}{|\mathbf{k}|^2-|\mathbf{p}|^2}\frac{\hat{R}(\mathbf{k}-\mathbf{p})}{(2\pi)^3}d\mathbf{p} \\ \sigma_a(\mathbf{k}) &= \int_{\mathbb{R}^3} \sigma(\mathbf{k},\mathbf{p})\Big(\frac{1+|\phi(\mathbf{x},\mathbf{p}-\mathbf{k})|^2}{2}-\phi(\mathbf{x},\mathbf{p}-\mathbf{k})\Big)\delta(c_0(|\mathbf{k}|-|\mathbf{p}|))d\mathbf{p}. \end{aligned} \tag{3.5}$$

The integral in the definition of $\Pi(\mathbf{k})$ has to be taken in the principal value sense. We assume that $\hat{R}(\mathbf{p})$ is sufficiently smooth and decays sufficiently fast at infinity so that the above integrals make sense. When $\phi \equiv 1$ we clearly recover (2.13). The main novelty in the above equation is the presence of the terms $\Pi(\mathbf{k})$ and $\sigma_a(\mathbf{k})$.

We postpone the derivation of the above modified radiative transfer equations to section 5. Their interpretation is as follows. Radiative transfer equations model how propagating modes are influenced by repeated interactions with weakly fluctuating inhomogeneities. In the weak fluctuation regime, each interaction is well described by its Born (linear) approximation [27, 28]. Roughly speaking, the terms in (3.5) that are quadratic in ϕ model the correlation of two paths interacting with fluctuations of κ_2, the terms linear in ϕ the correlation of one path interacting with κ_1 and one with κ_2, whereas the terms independent of ϕ involve interactions with κ_1 only.

Notice that the signal $\mathbf{u}^B(\boldsymbol{\xi};\mathbf{x}_0)$ given through (2.12) is still real-valued, as is expected physically. Indeed, to obtain the Fourier transform of a real-valued signal in (2.12), it is sufficient to show that

$$a_\pm^*(-\mathbf{k}) = a_\mp(\mathbf{k}) \qquad \text{since} \qquad S_\pm^*(-\mathbf{k}) = S_\mp(\mathbf{k}).$$

We deduce from (3.3) and from the relations $\sigma(-\mathbf{p},-\mathbf{k}) = \sigma(\mathbf{p},\mathbf{k})$ and $\hat{R}(\mathbf{k}) = \hat{R}(-\mathbf{k})$ that $a_\pm^*(-\mathbf{k})$ and $a_\mp(\mathbf{k})$ satisfy the same equation (3.4), hence are equal. Notice also that inelastic scattering now also occurs as the term $\Pi(\mathbf{k})$ no longer involves an integration over the shell $\delta(c_0(|\mathbf{k}|-|\mathbf{p}|))$.

3.3. Analysis in simple environment changes. Let us see how the solution of the transport equation (3.4) and the constitutive parameters (3.5) vary in simplified cases. A quantification of the impact that these modifications imply on the back-propagated signal given by (2.12) is postponed to section 4 devoted to the diffusive regime. In that regime, the formula (2.12) simplifies substantially so that the main effects arising from changes in the underlying environment are easier to describe.

Let us first consider the case $\phi(\mathbf{x},\mathbf{k}) = \phi(\mathbf{k})$ independent of $\mathbf{x}$ and $|\phi(\mathbf{k})|$ is invariant by rotation, in the sense that for all rotation $\mathcal{R}$, we have $|\phi(\mathbf{k})| = |\phi(\mathcal{R}\mathbf{k})|$. This implies that $\Pi(\mathbf{k}) = \Pi(|\mathbf{k}|)$. Since $|\mathbf{k}|$ is preserved by the scattering operator Q (in the sense that if $a(\mathbf{k})$ is supported on the shell $|\mathbf{k}| = k_0$, then so is $Qa(\mathbf{k})$), we can verify that

$$\tilde{a}_\pm(t,\mathbf{x},\mathbf{k}) = e^{\pm i\Pi(|\mathbf{k}|)t}a_\pm(t,\mathbf{x},\mathbf{k}) \tag{3.6}$$

satisfies the same equation (3.4) where $\Pi(|\mathbf{k}|)$ is now replaced by 0. When $|\phi| \not\equiv 1$, i.e. when the intensities of the fluctuations κ_1 and κ_2 differ, we see that a first effect of the changing environment is a modulation in time of the filters $a_\pm(t,\mathbf{x},\mathbf{k})$.

Another interesting case in practice is when $\phi(\mathbf{x},\mathbf{k}) = \phi(\mathbf{x})$, which is thus real-valued thanks to (3.3). We then observe that σ_a is real-valued. The scattering term

$Qa_\pm$ is not very different from that in (2.13) except for the multiplicative factor $\phi(\mathbf{x})$. The new term $\sigma_a a_\pm$ however is purely *absorbing*. Therefore, an effective absorption term is introduced as ϕ departs from the value 1. The constructive interferences, which build up in the time reversal experiment to create enhanced refocusing properties, are progressively diminished as κ_2 moves away from κ_1.

Let us finally consider the case $\phi(\mathbf{x},\mathbf{k}) = e^{i\mathbf{k}\cdot\boldsymbol{\tau}}$. This corresponds to shifting the medium by $\boldsymbol{\tau}$ before back-propagating the signal and may correspond to a ship drifting on the ocean surface before the time reversed signal is emitted. We observe here that $\Pi(\mathbf{k}) = 0$ and that $\sigma_a(\mathbf{k})$ is no longer real-valued. Let us introduce

$$\bar{a}_\pm(t,\mathbf{x},\mathbf{k}) = e^{i\mathbf{k}\cdot\boldsymbol{\tau}} a_\pm(t,\mathbf{x},\mathbf{k}). \tag{3.7}$$

It is then straightforward to verify that $\bar{a}_\pm$ satisfies the same equation (2.13) but with initial conditions given by

$$\bar{a}_\pm(t,\mathbf{x},\mathbf{k}) = e^{i\mathbf{k}\cdot\boldsymbol{\tau}}|\chi(\mathbf{x})|^2.$$

This implies that the *intensity* $|\chi(\mathbf{x})|^2$ of the detectors is modulated in the phase space. Coherence is therefore again partly lost and the refocused signal has a decreased intensity as $|\boldsymbol{\tau}|$ increases, at least for small values of $|\boldsymbol{\tau}|$.

4. Time Reversal in Diffusive Regime. The relation (2.12) shows that the whole time reversal experiment is described by the behavior of the modes $a_\pm(t,\mathbf{x},\mathbf{k})$. These modes are more easily described in the *diffusive* regime, which corresponds to a high scattering approximation of the transport regime.

4.1. Case of fixed media. It is well known that the solution to the radiative transfer equations (2.13) is well-approximated by the solution to a diffusion equation in the regime of high scattering [13, 24, 27]. Let us define the mean free path as $l = c_0/\Sigma$, where Σ is given by (2.16). It can be understood as the main distance between successive interactions of the modes $a_\pm$ with the underlying medium. The diffusive regime arises when $\eta = l/L \ll 1$. If time and space are rescaled appropriately as $t \to t/\eta^2$ and $\mathbf{x} \to \mathbf{x}/\eta$, we obtain in the limit that the propagating modes are independent of the direction of propagation so that

$$a_\pm(t,\mathbf{x},\mathbf{k}) \approx a(t,\mathbf{x},|\mathbf{k}|),$$

where

$$\begin{aligned} &\frac{\partial a}{\partial t} - D(|\mathbf{k}|)\Delta_{\mathbf{x}} a = 0 \\ &a(0,\mathbf{x},|\mathbf{k}|) = \frac{c_0}{4\pi|\mathbf{k}|^2}\int_{\mathbb{R}^3} a_\pm(0,\mathbf{x},\mathbf{p})\delta(c_0(|\mathbf{k}|-|\mathbf{p}|))d\mathbf{p}. \end{aligned} \tag{4.1}$$

The diffusion coefficient is given by

$$D(|\mathbf{k}|) = \frac{c_0^2}{3[\Sigma(|\mathbf{k}|) - \lambda(|\mathbf{k}|)]}, \tag{4.2}$$

where λ is such that [27]

$$\lambda(|\mathbf{k}|)\hat{\mathbf{k}} = \frac{c_0^2|\mathbf{k}|^2}{(4\pi)^2}\int_{\mathbb{R}^3} \hat{R}(\mathbf{p}-\mathbf{k})\hat{\mathbf{p}}\delta(c_0(|\mathbf{k}|-|\mathbf{p}|))d\mathbf{p}. \tag{4.3}$$

As in the transport case, $|\mathbf{k}|$ is a parameter in the above equation and solutions $a(t,\mathbf{x},|\mathbf{k}|)$ at different values of $|\mathbf{k}|$ satisfy decoupled equations.

Using the above results and (2.12), we deduce that the back-propagated pressure field is given in the diffusive regime by

$$\hat{p}^B(\mathbf{k};\mathbf{x}_0) = a(T,\mathbf{x}_0,|\mathbf{k}|)\hat{p}_0(\mathbf{k}), \tag{4.4}$$

when $g(\mathbf{x}) = 0$. In this regime, the time reversal experiment is thus interpreted as follows. We solve a diffusion equation with initial conditions given by the intensity of the detectors $a(0,\mathbf{x},|\mathbf{k}|) = |\chi(\mathbf{x})|^2$; see (2.13). Then $a(T,\mathbf{x}_0,|\mathbf{k}|)$ provides the filter indicating how a localized source term in the vicinity of $\mathbf{x}_0$ with wavenumber $\mathbf{k}/\varepsilon$ (reduced wavenumber $\mathbf{k}$) is amplified by a time reversal experiment where forward and backward fields propagate for a duration equal to T.

4.2. Case of changing media. The above result can be extended to the case of changing media. We assume to simplify that the change of underlying media is modeled by

$$\phi(\mathbf{k}) = |\phi| e^{i\boldsymbol{\tau}\cdot\mathbf{k}}. \tag{4.5}$$

This models modifications in the intensity and shifting of the heterogeneities. Both modifications could more generally have a spatial dependence. However the resulting diffusion equations have a much more cumbersome expression that we do not consider here. It is useful to realize that the the radiative transfer equation (3.4) may be recast in this setting as

$$\begin{aligned} &\Big(\frac{\partial}{\partial t} \pm c_0\hat{\mathbf{k}}\cdot\nabla \pm i\Pi(|\mathbf{k}|)\Big)a_\pm + \Sigma_\phi(|\mathbf{k}|)a_\pm = (K_\phi a_\pm)(t,\mathbf{x},\mathbf{k}),\\ &a_\pm(0,\mathbf{x},\mathbf{k}) = |\chi(\mathbf{x})|^2, \end{aligned} \tag{4.6}$$

where

$$\begin{aligned} \Sigma_\phi(|\mathbf{k}|) &= \frac{1+|\phi|^2}{2}\Sigma(|\mathbf{k}|)\\ K_\phi a(\mathbf{k}) &= e^{-i\boldsymbol{\tau}\cdot\mathbf{k}}|\phi|\int_{\mathbb{R}^3}\sigma(\mathbf{k},\mathbf{p})e^{i\boldsymbol{\tau}\cdot\mathbf{p}}a(\mathbf{p})\delta(c_0(|\mathbf{k}|-|\mathbf{p}|))d\mathbf{p}. \end{aligned}$$

To be consistent with the diffusive regime, we assume that

$$|\phi| = (1+\eta\psi), \tag{4.7}$$

where ψ is a parameter of order $O(1)$. We also rescale the array of detectors such that

$$\chi(\frac{\mathbf{x}}{\eta}) = \tilde{\chi}(\mathbf{x}), \tag{4.8}$$

independent of the scaled mean free path η. This is consistent with the initial conditions obtained in the preceding section 4.1.

We consider the approximation of a_+, to fix ideas, in the diffusive regime. We know that with (4.5), $\Pi(\mathbf{k}) = \Pi(|\mathbf{k}|)$ generates a modulation in time. We also want to compensate for the shift $\boldsymbol{\tau}$ and assuming that $|\mathbf{k}|$ is fixed introduce the following ansatz

$$a_+(t,\mathbf{x},|\mathbf{k}|\hat{\mathbf{k}}) = a(\eta^2 t,\eta\mathbf{x},\hat{\mathbf{k}})e^{-i\Pi(|\mathbf{k}|)(\eta^2 t)/\eta^2}e^{-i\boldsymbol{\tau}\cdot\mathbf{k}}. \tag{4.9}$$

Using the above notation, the equation for a is then

$$\begin{aligned} &\eta\frac{\partial a}{\partial t} + c_0\hat{\mathbf{k}}\cdot\nabla a + \frac{\eta\psi^2\Sigma}{2}a = \frac{|\phi|}{\eta}Qa \\ &a(0,\mathbf{x},\hat{\mathbf{k}}) = e^{i\Pi(|\mathbf{k}|)t/\eta^2}e^{i\boldsymbol{\tau}\cdot\mathbf{k}}|\tilde{\chi}(\mathbf{x})|^2, \end{aligned} \tag{4.10}$$

where the operator Q is defined here as

$$Qa(\hat{\mathbf{k}}) = \int_{\mathbb{R}^3}\sigma(\mathbf{k},\mathbf{p})(a(\hat{\mathbf{p}}) - a(\hat{\mathbf{k}}))\delta(c_0(|\mathbf{k}| - |\mathbf{p}|))d\mathbf{p}.$$

This equation has essentially the same form as (2.13) with an additional absorption term proportional to ψ^2. The derivation of a diffusion approximation for a is then classical [13]. We assume that $a = a_0 + \eta a_1 + \eta^2 a_2$, plug this ansatz into the transport equation (4.10) and equate like powers of η. At the first order we find that $a_0 = a_0(t,\mathbf{x})$ independent of $\hat{\mathbf{k}}$. The second equation yields that

$$a_1(t,\mathbf{x},\hat{\mathbf{k}}) = \frac{-c_0}{\Sigma(|\mathbf{k}|) - \lambda(|\mathbf{k}|)}\hat{\mathbf{k}}\cdot\nabla a_0(t,\mathbf{x}),$$

where λ is defined in (4.3). Upon averaging the third equation over S^2, we deduce that

$$\begin{aligned} &\frac{\partial a_0}{\partial t} + \frac{\Sigma(|\mathbf{k}|)\psi^2}{2}a_0 - D(|\mathbf{k}|)\Delta a_0 = 0, \\ &e^{-i\Pi(|\mathbf{k}|)t/\eta^2}a_0(0,\mathbf{x}) = |\tilde{\chi}(\mathbf{x})|^2\frac{1}{4\pi}\int_{S^2}e^{i\boldsymbol{\tau}\cdot\mathbf{k}}d\hat{\mathbf{k}} = |\tilde{\chi}(\mathbf{x})|^2\frac{\sin|\boldsymbol{\tau}||\mathbf{k}|}{|\boldsymbol{\tau}||\mathbf{k}|}. \end{aligned} \tag{4.11}$$

The diffusion coefficient $D(|\mathbf{k}|)$ is still given by (4.2). This diffusion equation is the main result of this section. It indicates how one can approximate the filter $a_+(T,\mathbf{x}_0,\mathbf{k})$ in (2.12) in the diffusive regime. The approximation for a_- is obtained by replacing c_0 by $-c_0$. Thus only the sign of Π in the phase term is changed.

4.3. Expression for the modes $a_\pm(t,\mathbf{x},\mathbf{k})$ in the diffusive regime. The diffusive regime allows us to obtain an intuitive idea of how refocusing is modified by changes in the underlying medium. Let us denote by $a(T,\mathbf{x}_0,|\mathbf{k}|)$ the filter obtained in a fixed medium corresponding to $\phi \equiv 1$. This is the solution to (4.1) with initial condition $a(0,\mathbf{x},|\mathbf{k}|) = |\tilde{\chi}(\mathbf{x})|^2$. It is then straightforward to realize that the modes $a_\pm$ obtained from solving the above diffusion equation (4.11) are given by

$$a_\pm(T,\mathbf{x}_0,\mathbf{k}) = e^{-i\boldsymbol{\tau}\cdot\mathbf{k}}\frac{\sin|\boldsymbol{\tau}||\mathbf{k}|}{|\boldsymbol{\tau}||\mathbf{k}|}e^{\mp i\Pi(|\mathbf{k}|)T/\eta^2}e^{-\Sigma(|\mathbf{k}|)\psi^2T/2}a(T,\mathbf{x}_0,|\mathbf{k}|). \tag{4.12}$$

Classical techniques [13] show that the error in proportional to η, for instance in the L^2 sense.

All the above terms are independent of the mean free path η except for the phase term $e^{\mp i\Pi(|\mathbf{k}|)T/\eta^2}$, which has not been rescaled yet. We may leave this term unscaled though this would correspond to a very oscillatory refocused signal as time T varies. We may also consider regimes in which the phase shift is of order $O(1)$ as well. We observe that

$$\frac{\Pi(|\mathbf{k}|)}{\eta^2} = \frac{-2\psi - \eta\psi^2}{\eta}\int_{\mathbb{R}^3}\frac{c_0}{2}\frac{|\mathbf{k}||\mathbf{p}|^2}{|\mathbf{k}|^2 - |\mathbf{p}|^2}\frac{\hat{R}(\mathbf{k}-\mathbf{p})}{(2\pi)^3}d\mathbf{p} \equiv \frac{-2\psi - \eta\psi^2}{\eta}\Pi_0(|\mathbf{k}|).$$

The phase term $e^{\mp i\Pi(|\mathbf{k}|)T/\eta^2}$ is thus highly oscillatory unless $\psi\Pi_0(|\mathbf{k}|)$ is of order η. This can be realized by assuming that ψ is of order η, in which case the absorption term $e^{-\Sigma(|\mathbf{k}|)\psi^2 T/2}$ becomes negligible in a first approximation. This can also be obtained if $\Pi_0(|\mathbf{k}|)$ is of order η. We can verify for instance that $\Pi_0(|\mathbf{k}|)$ can be made arbitrarily small by choosing a constant power spectrum $\hat{R}(\mathbf{p})$ on a disc of radius k_m much smaller than $|\mathbf{k}|$. In that case, we still verify that the diffusion coefficient D and the total cross section Σ are of order $O(1)$. There are therefore situations in which the modulation term $\Pi(\mathbf{k})/\eta^2$ is of order $O(1)$ and we consequently introduce the notation

$$\frac{\Pi(|\mathbf{k}|)}{\eta^2} = \Pi_s(|\mathbf{k}|). \tag{4.13}$$

We assume that the rescaled quantity Π_s is of order $O(1)$.

4.4. Main result on Time Reversal refocusing in changing media. Collecting the simplifications introduced in the preceding sections, we finally deduce from (2.12) that the back-propagated signal in the diffusive regime takes the form

$$\begin{aligned}\hat{\mathbf{u}}^B(\mathbf{k};\mathbf{x}_0) = &\left[\begin{pmatrix}\sin(\Pi_s T)\sqrt{\dfrac{\kappa_0}{\rho}}i\hat{\mathbf{k}} \\ \cos(\Pi_s T)\end{pmatrix}\hat{p}_0(\mathbf{k}) + \begin{pmatrix}\cos(\Pi_s T)i\hat{\mathbf{k}} \\ -\sin(\Pi_s T)\sqrt{\dfrac{\rho}{\kappa_0}}\end{pmatrix}|\mathbf{k}|\hat{\varphi}(\mathbf{k})\right] \\ &\times e^{-i\boldsymbol{\tau}\cdot\mathbf{k}}\ \frac{\sin|\boldsymbol{\tau}||\mathbf{k}|}{|\boldsymbol{\tau}||\mathbf{k}|}\ e^{-\Sigma\psi^2 T/2}\ a(T,\mathbf{x}_0,|\mathbf{k}|).\end{aligned} \tag{4.14}$$

This is to be compared to the case where $\Pi_s = \psi = |\boldsymbol{\tau}| = 0$ when the medium remains the same during the forward and backward propagations. The above formula emphasizes two principal distinct effects that appear when the back-propagation occurs in a different underlying medium.

4.5. Modified fluctuations amplitude. When the amplitude of the fluctuations is multiplied by $\phi = 1+\psi$, We observe two effects. First, the refocused signal is exponentially damped by an amount equal to $e^{-\Sigma\psi^2 T/2}$. Secondly, such fluctuations generate a phase modulation in the duration variable T: an initial pressure field generates a back-propagated pressure field multiplied by $\cos(\Pi_s T)$ and a velocity field proportional to $\sin(\Pi_s T)$, and vice-versa for an initial velocity field.

This implies a transfer from potential energy to kinetic energy and vice-versa. At $T = \pi\Pi_s^{-1}/2$ for instance, a signal with no kinetic energy initially ($\nabla\varphi = \mathbf{0}$) will generate a back-propagated signal with no potential energy ($p^B(\boldsymbol{\xi};\mathbf{x}_0) = 0$).

Notice that in the experimental setting where the signals are recorded in time [17, 23], the back-propagated signal will have the same form as in (4.14), but averaged in time. As a consequence the back-propagated signal may be extremely faint when the signal is recorded at the detector array over a long time compared to $|\Pi_s|^{-1}$. A possible remedy would be to multiply the signal at the detectors by a function of T. For instance one could choose

$$\chi(\mathbf{x};T) = \begin{cases}\chi(\mathbf{x}) & \cos\Pi_s T > 0 \\ 0 & \cos\Pi_s T \le 0.\end{cases}$$

This would allow us to obtain a much larger back-propagated signal even for recording durations large compared to $|\Pi_s|^{-1}$. This however requires to *know* in advance the modulation frequency Π_s.

4.6. Drifting environment. The second effect we wish to emphasize is the following. When the medium is shifted by an amount $\boldsymbol{\tau}$, the time reversal filter first accounts for the shift by multiplying the source term in the Fourier domain by the corresponding phase $e^{-i\boldsymbol{\tau}\cdot\mathbf{k}}$. In the physical domain, this means that the back-propagated signal will refocus at a location $\boldsymbol{\tau}$ away from the original source term since $e^{i\boldsymbol{\tau}\cdot\mathbf{k}}\hat{\mathbf{u}}^B(\mathbf{k};\mathbf{x}_0)$ is the Fourier transform of $\mathbf{u}^B(\boldsymbol{\xi}+\boldsymbol{\tau};\mathbf{x}_0)$. Moreover this shift is accompanied by a decoherence of the refocusing signal, which translates in the diffusive regime after averaging over all directions, into a modulation of the amplitude by a sinc (cardinal sine) function.

We therefore obtain the seemingly striking result that a shift by

$$|\boldsymbol{\tau}| = \frac{\pi}{|\mathbf{k}|} = \frac{\lambda}{2}$$

completely cancels the back-propagated signal. This phenomenon is similar to the well-known fact that the correlation $\langle p(\mathbf{x})p(\mathbf{x}+\lambda\hat{\boldsymbol{\tau}}/2)\rangle$ of a wavefield at two points separated by $\lambda/2$ (with $\hat{\boldsymbol{\tau}}$ an arbitrary unit vector) vanishes in the diffusive regime.

5. Derivation of transport equations in moving media. This section is devoted to the derivation of (3.4), which describes the effects of changing the underlying medium before re-emitting the time reversed signal. Since the derivation of radiative transfer equations itself is rather complicated when wave propagation is modeled by a first-order system of the form (2.4), we first focus here on a simpler scalar model based on the Schrödinger equation. The generalization to first-order hyperbolic systems is postponed to the end of the section.

In the weak coupling regime, the regime of interest in this paper, the Schrödinger equation takes the form [27]

$$\frac{\partial\psi_\varepsilon}{\partial t}(t,\mathbf{x}) = \frac{i\varepsilon}{2}\Delta\psi_\varepsilon(t,\mathbf{x}) - \frac{i}{\sqrt{\varepsilon}}V_j(\frac{\mathbf{x}}{\varepsilon})\psi_\varepsilon(t,\mathbf{x}), \tag{5.1}$$

for $j=1,2$, where $j=1$ corresponds to the medium during the forward propagation and $j=2$ to the medium during the backward propagation after time reversal. Here the potentials $V_{1,2}$ play the same role as $\kappa_{1,2}$ in earlier sections. We assume that they are mean-zero stationary random processes. We define the two point correlation functions

$$R_{mn}(\mathbf{x}) = \langle V_m(\mathbf{y})V_n(\mathbf{y}+\mathbf{x})\rangle, \qquad m,n=1,2, \tag{5.2}$$

and the power spectra $\hat{R}_{mn}(\mathbf{k})$ by their Fourier transforms.

As is shown in several works on time reversal [5, 6, 10] the filter relating the source term to the back-propagated signal as in (2.12) is given by the limit as $\varepsilon\to 0$ of the following *Wigner transform*

$$W_\varepsilon(t,\mathbf{x},\mathbf{k}) = \int_{\mathbb{R}^3} e^{i\mathbf{k}\cdot\mathbf{y}}\psi_{f\varepsilon}(t,\mathbf{x}-\frac{\varepsilon\mathbf{y}}{2})\psi^*_{b\varepsilon}(t,\mathbf{x}+\frac{\varepsilon\mathbf{y}}{2})\frac{d\mathbf{y}}{(2\pi)^3}. \tag{5.3}$$

Here $\psi_{f\varepsilon}$ and $\psi_{b\varepsilon}$ solve (5.1) with forward potential $V=V_1$ and backward potential $V=V_2$, respectively, with suitable initial conditions [6]. When $V_1\equiv V_2$ so that the underlying medium is not modified before back-propagation, it is well known [16, 27] that the high frequency limiting equation is precisely a radiative transfer equation of the form

$$\frac{\partial W}{\partial t} + \mathbf{k}\cdot\nabla W = \int_{\mathbb{R}^3}\hat{R}(\mathbf{p}-\mathbf{k})(W(t,\mathbf{x},\mathbf{p})-W(t,\mathbf{x},\mathbf{k}))\delta(\frac{|\mathbf{p}|^2-|\mathbf{k}|^2}{2})\frac{d\mathbf{p}}{(2\pi)^2}. \tag{5.4}$$

In the case of acoustic waves, the above limiting equation is replaced by (2.13). We now present how the above equation should be modified when $V_2 \neq V_1$. In the acoustics case, this generalizes to (3.4).

Our derivation follows the framework in [7, 27]. First we obtain that W_ε solves the following equation:

$$\frac{\partial W_\varepsilon}{\partial t} + \mathbf{k}\cdot\nabla W_\varepsilon = \int_{\mathbb{R}^3} K_\varepsilon(\mathbf{x},\mathbf{k}-\mathbf{p})W_\varepsilon(t,\mathbf{x},\mathbf{p})d\mathbf{p}, \tag{5.5}$$

where the convolution kernel K_ε is given by

$$K_\varepsilon(\mathbf{x},\mathbf{p}) = \frac{1}{i\pi^3\sqrt{\varepsilon}}\Big(\hat{V}_1(2\mathbf{p})e^{i2\mathbf{p}\cdot\mathbf{x}/\varepsilon} - \hat{V}_2(-2\mathbf{p})e^{-i2\mathbf{p}\cdot\mathbf{x}/\varepsilon}\Big). \tag{5.6}$$

Inverting the free transport operator $\partial_t + \mathbf{k}\cdot\nabla$ we obtain that

$$W_\varepsilon(t,\mathbf{x},\mathbf{k}) = W_\varepsilon(0,\mathbf{x}-t\mathbf{k},\mathbf{k}) + \int_0^t\int K_\varepsilon(\mathbf{x}-s\mathbf{k},\mathbf{k}-\mathbf{p})W_\varepsilon(t-s,\mathbf{x}-s\mathbf{k},\mathbf{p})d\mathbf{p}ds.$$

After one more iteration we have

$$\begin{aligned}
&W_\varepsilon(t,\mathbf{x},\mathbf{k}) = W_\varepsilon(0,\mathbf{x}-t\mathbf{k},\mathbf{k})\\
&+\int_0^t\int K_\varepsilon(\mathbf{x}-s\mathbf{k},\mathbf{k}-\mathbf{p})W_\varepsilon(0,\mathbf{x}-s\mathbf{k}-(t-s)\mathbf{p},\mathbf{p})d\mathbf{p}ds\\
&+\int_0^t\int K_\varepsilon(\mathbf{x}-s\mathbf{k},\mathbf{k}-\mathbf{p})\int_0^{t-s}\int K_\varepsilon(\mathbf{x}-s\mathbf{k}-u\mathbf{p},\mathbf{p}-\mathbf{q})\\
&\qquad\times W_\varepsilon(t-s-u,\mathbf{x}-s\mathbf{k}-u\mathbf{p},\mathbf{q})d\mathbf{q}dud\mathbf{p}ds.
\end{aligned} \tag{5.7}$$

We now average the above equation with respect to the realizations of the random medium. We assume that $\langle K_\varepsilon\otimes K_\varepsilon W_\varepsilon\rangle = \langle K_\varepsilon\otimes K_\varepsilon\rangle\langle W_\varepsilon\rangle$ and that W_ε is sufficiently smooth. Such assumptions cannot be justified at this level although they are known to provide the correct results [5, 16, 27].

Using that

$$\langle \hat{V}_m(\mathbf{p})\hat{V}_n(\mathbf{q})\rangle = (2\pi)^3\hat{R}_{mn}(\mathbf{p})\delta(\mathbf{p}+\mathbf{q}), \qquad m,n=1,2,$$

which comes from taking Fourier transforms in (5.2), we deduce that

$$\begin{aligned}
&\langle K_\varepsilon(\mathbf{y},\mathbf{k}-\mathbf{p})K_\varepsilon(\mathbf{y}-u\mathbf{p},\mathbf{p}-\mathbf{q})\rangle = \frac{-1}{\pi^3\varepsilon}\\
&\times\Big(\quad \hat{R}_{11}(2(\mathbf{k}-\mathbf{p}))e^{2i(\mathbf{k}-\mathbf{p})\cdot\mathbf{p}u/\varepsilon}\delta(\mathbf{k}-\mathbf{q})\\
&\quad - \hat{R}_{12}(2(\mathbf{k}-\mathbf{p}))e^{2i(\mathbf{k}-\mathbf{p})\cdot\mathbf{p}u/\varepsilon}\delta(\mathbf{k}+\mathbf{q}-2\mathbf{p})\\
&\quad - \hat{R}_{21}(-2(\mathbf{k}-\mathbf{p}))e^{-2i(\mathbf{k}-\mathbf{p})\cdot\mathbf{p}u/\varepsilon}\delta(\mathbf{k}+\mathbf{q}-2\mathbf{p})\\
&\quad + \hat{R}_{22}(2(\mathbf{k}-\mathbf{p}))e^{-2i(\mathbf{k}-\mathbf{p})\cdot\mathbf{p}u/\varepsilon}\delta(\mathbf{k}-\mathbf{p})\qquad\Big).
\end{aligned}$$

The power spectrum $\hat{R}_{mn}$ is a 2×2 positive definite matrix such that $\hat{R}_{mn}(-\mathbf{p}) = \hat{R}_{nm}(\mathbf{p})$, $m,n=1,2$. After the changes of variables $2\mathbf{p}-\mathbf{k}\to\mathbf{p}$ and $u\to\varepsilon u$ and replacing $W_\varepsilon(t-s-\varepsilon u,\mathbf{x}-s\mathbf{k}-\varepsilon u\mathbf{p},\mathbf{q})$ by $W_\varepsilon(t-s,\mathbf{x}-s\mathbf{k},\mathbf{q})$ we deduce that the ensemble average of the last term in (5.7) is approximated by

$$\begin{aligned}
&\int_0^t\int\int_0^{(t-s)/\varepsilon} \\
&\times\Big(-e^{iu\frac{|\mathbf{k}|^2-|\mathbf{p}|^2}{2}}R_{11}(\mathbf{p}-\mathbf{k}) - e^{-iu\frac{|\mathbf{k}|^2-|\mathbf{p}|^2}{2}}R_{22}(\mathbf{p}-\mathbf{k})\Big)\langle W_\varepsilon\rangle(t-s,\mathbf{x}-s\mathbf{k},\mathbf{k})\\
&+\Big(e^{iu\frac{|\mathbf{k}|^2-|\mathbf{p}|^2}{2}} + e^{-iu\frac{|\mathbf{k}|^2-|\mathbf{p}|^2}{2}}\Big)R_{21}(\mathbf{p}-\mathbf{k})\langle W_\varepsilon\rangle(t-s,\mathbf{x}-s\mathbf{k},\mathbf{p})\frac{dud\mathbf{p}ds}{(2\pi)^3}.
\end{aligned} \tag{5.8}$$

We now pass to the limit $\varepsilon \to 0$ and replace $\langle W_\varepsilon \rangle$ by its limit W. We first observe that

$$\int_0^\infty e^{\pm iu\omega} du = \pi\delta(\omega) \pm \frac{i}{\omega}.$$

Thus in the limit $\varepsilon \to 0$ we obtain the equation

$$\begin{aligned} & W(t,\mathbf{x},\mathbf{k}) = W(0,\mathbf{x}-t\mathbf{k},\mathbf{k}) + \int_0^t \\ & \Big(\int \hat{R}_{21}(\mathbf{p}-\mathbf{k}) W(t-s,\mathbf{x}-s\mathbf{k},\mathbf{p}) \delta(\frac{|\mathbf{k}|^2-|\mathbf{p}|^2}{2}) \frac{d\mathbf{p}}{(2\pi)^2} \\ & \quad -(\Sigma(\mathbf{k}) + i\Pi(\mathbf{k})) W(t-s,\mathbf{x}-s\mathbf{k},\mathbf{k}) \Big) ds, \end{aligned} \tag{5.9}$$

where the total absorption and phase modulation terms are given by

$$\begin{aligned} \Sigma(\mathbf{k}) &= \int \frac{\hat{R}_{11}(\mathbf{p}-\mathbf{k}) + \hat{R}_{22}(\mathbf{p}-\mathbf{k})}{2} \delta(\frac{|\mathbf{k}|^2-|\mathbf{p}|^2}{2}) \frac{d\mathbf{p}}{(2\pi)^2} \\ \Pi(\mathbf{k}) &= \fint \Big(\hat{R}_{11}(\mathbf{p}-\mathbf{k}) - \hat{R}_{22}(\mathbf{p}-\mathbf{k}) \Big) \frac{2}{|\mathbf{k}|^2-|\mathbf{p}|^2} \frac{d\mathbf{p}}{(2\pi)^3}. \end{aligned} \tag{5.10}$$

The latter integral defining Π has to be understood in the principal value sense. We assume that the power spectrum $\hat{R}_{mn}$ is such that the above integrals exist. This is the integral formulation of the following radiative transfer equation

$$\begin{aligned} & \frac{\partial W}{\partial t} + \mathbf{k}\cdot\nabla W + (\Sigma(\mathbf{k}) + i\Pi(\mathbf{k}))W \\ & \qquad = \int \hat{R}_{21}(\mathbf{p}-\mathbf{k}) W(t,\mathbf{x},\mathbf{p}) \delta(\frac{|\mathbf{k}|^2-|\mathbf{p}|^2}{2}) \frac{d\mathbf{p}}{(2\pi)^2}. \end{aligned} \tag{5.11}$$

This equation generalizes (5.4) in the case of changing environments.

Let us now assume that $\hat{V}_1(\mathbf{k}) = \hat{V}(\mathbf{k})$ and $\hat{V}_2(\mathbf{k}) = \phi(\mathbf{k})\hat{V}_1(\mathbf{k})$, where $\phi(\mathbf{k})$ is a deterministic function as in sections 3 and 4. We then obtain that $\hat{R}_{11}(\mathbf{p}) = \hat{R}(\mathbf{p})$, $\hat{R}_{22}(\mathbf{p}) = |\phi(\mathbf{p})|^2\hat{R}(\mathbf{p})$, and $\hat{R}_{21}(\mathbf{p}) = \phi(\mathbf{p})\hat{R}(\mathbf{p})$, where $\hat{R}(\mathbf{p})$ is the power spectrum associated with the random field $V(\mathbf{x})$. We thus finally recast (5.11) as follows

$$\frac{\partial W}{\partial t} + \mathbf{k}\cdot\nabla W + (\sigma_a(\mathbf{k}) + i\Pi(\mathbf{k}))W = QW, \tag{5.12}$$

where

$$\begin{aligned} & QW(t,\mathbf{x},\mathbf{k}) = \int \hat{R}(\mathbf{p}-\mathbf{k})\phi(\mathbf{p}-\mathbf{k}) \Big[W(t,\mathbf{x},\mathbf{p}) - W(t,\mathbf{x},\mathbf{k}) \Big] \delta(\frac{|\mathbf{k}|^2-|\mathbf{p}|^2}{2}) \frac{d\mathbf{p}}{(2\pi)^2}, \\ & \sigma_a(\mathbf{k}) = \int \hat{R}(\mathbf{p}-\mathbf{k}) \Big(\frac{1+|\phi(\mathbf{p}-\mathbf{k})|^2}{2} - \phi(\mathbf{p}-\mathbf{k}) \Big) \delta(\frac{|\mathbf{k}|^2-|\mathbf{p}|^2}{2}) \frac{d\mathbf{p}}{(2\pi)^2} \\ & \Pi(\mathbf{k}) = \fint \hat{R}(\mathbf{p}-\mathbf{k}) \Big[1 - |\phi(\mathbf{p}-\mathbf{k})|^2 \Big] \frac{2}{|\mathbf{k}|^2-|\mathbf{p}|^2} \frac{d\mathbf{p}}{(2\pi)^3}. \end{aligned} \tag{5.13}$$

This explains how the equation for the Wigner transform generalizes when the medium in which back-propagation occurs changes. We verify that modulations of $\phi(\mathbf{x},\mathbf{k})$ at the macroscopic scale $\mathbf{x}$ do not change the interference results at the microscopic scale. We can thus replace formally $\phi(\mathbf{k})$ by $\phi(\mathbf{k},\mathbf{x})$. We do not dwell on the details.

In the case of acoustic waves, the dispersion relation is $\omega = \pm c_0|\mathbf{k}|$ depending on the propagating mode instead of $\omega = |\mathbf{k}|^2/2$. The group velocity is then $\pm c_0\hat{\mathbf{k}}$ instead of $\mathbf{k}$ and energy conservation through scattering is given by $\delta(\pm c_0(|\mathbf{k}| - |\mathbf{p}|))$ instead of $\delta((|\mathbf{k}|^2 - |\mathbf{p}|^2)/2)$. The presence of two propagating modes in the acoustic case compared to only one in the Schrödinger case, makes the derivation somewhat more delicate. A detailed derivation of (3.4) requires using the machinery developed in [27]. To avoid unnecessary repetitions, we use the notation of that paper and merely sketch the modifications that are required to deal with time reversal in changing environment. We refer to [27] for notation and details. Let us assume that $\rho = \kappa_0 = 1$ to simplify so that $\omega_\pm(\mathbf{k}) = \pm|\mathbf{k}|$ and $\omega_{1,2} = 0$. We define the eigenvectors $\mathbf{b}_\pm(\mathbf{k}) = 2^{-1/2}(\pm\hat{\mathbf{k}}, 1)$, where $\hat{\mathbf{k}} = \mathbf{k}/|\mathbf{k}|$ and $\mathbf{b}_{1,2}(\mathbf{k})$ as a basis for the vectors orthogonal to $\mathbf{b}_\pm(\mathbf{k})$. The Fourier transform $F^{(1)}(\mathbf{p},\mathbf{k})$ of the corrector $W^{(1)}(\boldsymbol{\xi},\mathbf{k})$ in [27, (4.21)] now takes the form

$$\begin{aligned} F^{(1)}(\mathbf{p},\mathbf{k}) &= \sum_{m,n} \frac{H_{m,n}(\mathbf{p},\mathbf{k})}{\omega_m(\mathbf{k}-\frac{\mathbf{p}}{2}) - \omega_n(\mathbf{k}+\frac{\mathbf{p}}{2}) + i\nu} \mathbf{b}_m(\mathbf{k}-\frac{\mathbf{p}}{2})\mathbf{b}_m^*(\mathbf{k}+\frac{\mathbf{p}}{2}) \\ H_{m,n}(\mathbf{p},\mathbf{k}) &= (\omega_m a_m)(\mathbf{k}+\frac{\mathbf{p}}{2})\frac{\hat{\kappa}_1(\mathbf{p})}{2} - (\omega_n a_n)(\mathbf{k}-\frac{\mathbf{p}}{2})\frac{\hat{\kappa}_2(\mathbf{p})}{2}. \end{aligned} \tag{5.14}$$

Here the sum in m and n runs over $\{+,-,1,2\}$. The modes $a_\pm$ are those defined in earlier sections and the modes $a_{1,2}$ are the non-propagating modes, which do not contribute eventually.

In order to derive the interaction operator we need to evaluate using the notation in [27, (4.23)] $(\mathcal{P}_2 + \mathcal{P}_1(\frac{\partial}{\partial\boldsymbol{\xi}}))W^{(1)}$. These operators are defined in [27, (4.15)] and [27, (4.16)], respectively. In time reversal in changing environment, the matrices $\hat{V}(\mathbf{q})$ and $\widehat{V^*}(\mathbf{q})$ that appear in those definitions need be replaced by

$$\hat{V}(\mathbf{q}) = \hat{\kappa}_1(\mathbf{q})\mathbf{e}_4 \otimes \mathbf{e}_4, \qquad \widehat{V^*}(\mathbf{q}) = \hat{\kappa}_2(\mathbf{q})\mathbf{e}_4 \otimes \mathbf{e}_4. \tag{5.15}$$

Notice that V^* is no longer the transpose matrix of V as in [27]. The evaluation of $(\mathcal{P}_2 + \mathcal{P}_1(\frac{\partial}{\partial\boldsymbol{\xi}}))W^{(1)}$ is then performed as in (5.8). The term proportional to $\delta(\omega_+(\mathbf{k}) - \omega_+(\mathbf{p}))$ is derived as in [27] and yields $Qa(\mathbf{k})$ and $\sigma_a(\mathbf{k})$ in (3.5). As in (5.9), there is an additional integral to be understood in the principal value sense, which here takes the form

$$i\sum_{m=\pm} \fint_{\mathbb{R}^3} (1 - |\phi(\mathbf{p}-\mathbf{k})|^2)\frac{\hat{R}(\mathbf{k}-\mathbf{p})}{4(2\pi)^3}\frac{\omega_+(\mathbf{k})\omega_m(\mathbf{p})a_+(\mathbf{k})}{\omega_m(\mathbf{p}) - \omega_+(\mathbf{k})}d\mathbf{p}.$$

After summation, this is $i\Pi(\mathbf{k})$ as defined in (3.5) for the forward propagating mode $a_+(t,\mathbf{x},\mathbf{k})$. This concludes the derivation of the modified equations.

6. Numerical Simulations. This section presents some numerical simulations that corroborate the theoretical predictions in (4.14). In order to lower the computational cost, we restrict ourselves to two-dimensional calculations in a periodic geometry. All calculations are thus performed on a box of size L^2.

6.1. Two dimensional setting. All the results obtained in earlier sections adapt to dimensions d greater than or equal to 2. Only in dimension $d = 1$ are the radiative transfer and diffusion limits not valid as energy tends to localize [1, 28]. For $d = 2$, radiative transfer equations can be justified [3, 16] with some quantitative modifications compared to the three dimensional case treated in earlier sections that we now explain. We still assume that the change of underlying media is modeled by (4.5) to simplify.

Several modifications are due to the inverse Fourier transform that reads for $d=2$ as

$$f(\mathbf{x}) = \frac{1}{(2\pi)^2}\int_{\mathbb{R}^2} e^{i\mathbf{x}\cdot\mathbf{k}}\hat{f}(\mathbf{k})d\mathbf{k}.$$

This implies that the power spectrum is now defined by

$$\langle \hat{\kappa}_1(\mathbf{p})\hat{\kappa}_1(\mathbf{q})\rangle = (2\pi)^2\kappa_0^2\hat{R}(\mathbf{p})\delta(\mathbf{p}+\mathbf{q}).$$

The scattering coefficient $\sigma(\mathbf{k},\mathbf{p})$ is given by

$$\sigma(\mathbf{k},\mathbf{p}) = \frac{\pi c_0^2}{2}|\mathbf{k}|^2\frac{\hat{R}(\mathbf{k}-\mathbf{p})}{(2\pi)^2} = \frac{c_0^2|\mathbf{k}|^2}{8\pi}\hat{R}(\mathbf{k}-\mathbf{p}), \tag{6.1}$$

and the total scattering coefficient by

$$\Sigma(|\mathbf{k}|) = \int_{\mathbb{R}^2}\sigma(\mathbf{k},\mathbf{p})\delta(c_0(|\mathbf{k}|-|\mathbf{p}|))d\mathbf{p} = \frac{c_0|\mathbf{k}|^3}{8\pi}\int_{S^1}\hat{R}(|\mathbf{k}||\hat{\mathbf{e}}-\hat{\mathbf{p}}|)d\hat{\mathbf{p}}, \tag{6.2}$$

with $\hat{\mathbf{e}}$ an arbitrary unit vector on the unit circle S^1. The coefficients defined in (3.5) are left unmodified except for the domain of integration, which is now $\mathbb{R}^2$. For the modulation term $\Pi(\mathbf{k})$ we thus obtain

$$\Pi(\mathbf{k}) = (1-|\phi|^2)\fint_{\mathbb{R}^2}\frac{c_0}{2}\frac{|\mathbf{k}||\mathbf{p}|^2}{|\mathbf{k}|^2-|\mathbf{p}|^2}\frac{\hat{R}(\mathbf{k}-\mathbf{p})}{(2\pi)^2}d\mathbf{p} \equiv (1-|\phi|^2)\Pi_0(\mathbf{k}). \tag{6.3}$$

The term $\Pi_0(\mathbf{k})$ thus depends only on the first medium characterized by $\kappa_1(\mathbf{x})$ and not on the second medium.

The diffusion equation (4.1) also remains valid. The initial conditions need be modified as

$$a(0,\mathbf{x},|\mathbf{k}|) = \frac{c_0}{2\pi|\mathbf{k}|}\int_{\mathbb{R}^2}a_\pm(0,\mathbf{x},\mathbf{p})\delta(c_0(|\mathbf{k}|-|\mathbf{p}|)d\mathbf{p},$$

and the diffusion coefficient is now given by [3]

$$\begin{aligned} D(|\mathbf{k}|) &= \frac{c_0^2}{2[\Sigma(|\mathbf{k}|)-\lambda(|\mathbf{k}|)]},\\ \lambda(|\mathbf{k}|)\hat{\mathbf{k}} &= \frac{c_0^2|\mathbf{k}|^2}{8\pi}\int_{\mathbb{R}^2}\hat{R}(\mathbf{p}-\mathbf{k})\hat{\mathbf{p}}\delta(c_0(|\mathbf{k}|-|\mathbf{p}|))d\mathbf{p}. \end{aligned} \tag{6.4}$$

This implies only one noticeable change in the expression for the propagating modes in the diffusive regime, namely the initial conditions in (4.11) now read

$$e^{-i\Pi(|\mathbf{k}|)t/\eta^2}a_0(0,\mathbf{x}) = |\tilde{\chi}(\mathbf{x})|^2\frac{1}{2\pi}\int_{S^1}e^{i\boldsymbol{\tau}\cdot\mathbf{k}}d\hat{\mathbf{k}} = |\tilde{\chi}(\mathbf{x})|^2 J_0(|\boldsymbol{\tau}||\mathbf{k}|), \tag{6.5}$$

where J_0 is the zero-th order Bessel function of the first kind. Therefore the main result (4.14) holds unchanged except for the sinc (cardinal sine) function that need be replaced by the Bessel function J_0. As a consequence, the back-propagated signal does not vanish for shifts such that $|\boldsymbol{\tau}| = n\lambda/2$ for $n\in\mathbb{N}^*$, but rather for values of $|\boldsymbol{\tau}|$ such that $|\boldsymbol{\tau}||\mathbf{k}|$ is a zero of J_0. Looking at tables of Bessel functions, one observes that the first two zeros occur for values of $|\boldsymbol{\tau}|$ equal to roughly 0.38λ and 0.89λ, respectively.

6.2. Calculations on a periodic box. Our numerical simulations solve (2.1) on a box $(0, L)^2$ with periodicity boundary conditions. Assuming that the density $\rho = 1$ to simplify, we observe that to leading order, we have

$$\frac{\delta\kappa(\mathbf{x})}{\kappa_0} \approx -\frac{\delta c^2(\mathbf{x})}{c_0^2}, \tag{6.6}$$

where we have written $c^2(\mathbf{x}) = c_0^2 + \delta c^2(\mathbf{x})$ and $\kappa(\mathbf{x}) = \kappa_0 + \delta\kappa(\mathbf{x})$. We thus concentrate on the definition of $\delta\kappa(\mathbf{x})$, which can be decomposed as

$$\delta\kappa(\mathbf{x}) = \sum_{\mathbf{m}\in\mathbb{Z}^2} \kappa_{\mathbf{m}} e^{i2\pi\mathbf{m}\cdot\mathbf{x}/L}. \tag{6.7}$$

In order to obtain (2.10) we need to ensure that

$$\langle \kappa_{\mathbf{n}}\kappa_{\mathbf{m}}\rangle = \langle|\kappa_{\mathbf{m}}|^2\rangle\delta(\mathbf{m}+\mathbf{n}). \tag{6.8}$$

This is achieved by introducing $\kappa_{\mathbf{m}} = |\kappa_{\mathbf{m}}|e^{i\varphi_{\mathbf{m}}}$, where $|\kappa_{\mathbf{m}}|$ are independent real-valued random variables, and $\varphi_{\mathbf{m}}$ are also independent random variables with uniform distribution on $(0, 2\pi)$. This implies that

$$\langle\delta\kappa(\mathbf{x})\delta\kappa(\mathbf{x}+\mathbf{y})\rangle = \sum_{\mathbf{m}\in\mathbb{Z}^2} \langle|\kappa_{\mathbf{m}}|^2\rangle e^{i2\pi\mathbf{m}\cdot\mathbf{y}/L},$$

independent of $\mathbf{x}$ as it should. When $L \to \infty$, we obtain in the limit the wave equation posed in the whole $\mathbb{R}^2$. From our definition of Fourier series and transforms we realize that

$$\hat{R}(\frac{2\pi\mathbf{m}}{L}) \approx L^2 R_{\mathbf{m}} = L^2\langle|\kappa_{\mathbf{m}}|^2\rangle.$$

In our numerical simulations we assume that $\hat{R}(\mathbf{k})$ is constant and given by κ^2 on a given domain Ω and vanishes outside this domain. The fluctuations in the compressibility $\kappa(\mathbf{x})$ are thus chosen such that $L^2\langle|\kappa_{\mathbf{m}}|^2\rangle = \kappa^2$ provided that $2\pi\mathbf{m}/L \in \Omega$ and $|\kappa_{\mathbf{m}}| = 0$ elsewhere. This is how the realizations of the random sound speed $c^2(\mathbf{x})$ are generated numerically using (6.6).

6.3. Numerical discretization. The wave equation (2.1) is solved as in [6] by using an explicit finite difference discretization of second order both in time and space (usual five-point stencil in space and three point stencil in time to discretize the second-order derivatives). The discretization parameters are $h = L/N_x$ and $\Delta t = T/N_t$. We also introduce $t_n = n\Delta t$. The value of the velocity field at the grid points $h\mathbf{n}$ is evaluated as indicated above. Notice that the resolution in time is time reversible, in the sense that the equations that yield $p(t_{n+1})$ from $p(t_{n-1})$ and $p(t_n)$ can be inverted to exactly retrieve $p(t_{n-1})$ from $p(t_n)$ and $p(t_{n+1})$. The time step Δt has been chosen small enough to ensure stability of the explicit scheme. In all our simulations we have chosen $N_x = 400$ and $c_0 \equiv 1$.

6.4. Numerical simulations. We have seen in (4.14) and more generally in (2.12) that the time reversal experiment is characterized by a filter at each wavenumber $\mathbf{k}$. To analyze this filter numerically, we consider initial conditions of the form $\hat{p}_0(\mathbf{k}) = \delta(\mathbf{k}-\mathbf{k}_0)$ and $\hat{\phi}(\mathbf{k}) = 0$. We then solve the wave equation with these initial conditions for a duration T. At time T we record the signal on the domain

$(L/3, 2L/3)^2$ to fix ideas. We choose the time T sufficiently large so that we are in the diffusive regime. The solution $a(T, \mathbf{x}, |\mathbf{k}|)$ to the diffusion equation in the periodic box then relaxes exponentially fast to a constant value $\bar{a}$ that corresponds to the initial energy captured by the detectors:

$$\bar{a} = \frac{1}{L^2}\int_{(0,L)^2} \chi^2(\mathbf{x})d\mathbf{x} = \frac{1}{L^2}\int_{(0,L)^2} e^{-20((\frac{2x}{L})^4+(\frac{2y}{L})^4)}dxdy \approx 0.1837. \qquad (6.9)$$

This implies that our choice of array, which is the same in each numerical simulation, records roughly 18% of the initial energy. We have verified that $(a(T, \mathbf{x}, |\mathbf{k}|) - \bar{a})/\bar{a}$ was less than 2% in the L^1 norm in all our numerical simulations. We then measure $e^{i\boldsymbol{\tau}\cdot\mathbf{k}_0}\hat{p}^B(\mathbf{k}_0)$. In practice this is done by calculating

$$F_{\text{data}} = \frac{(p^B(\mathbf{x}+\boldsymbol{\tau}), p_0(\mathbf{x}))}{\|p_0(\mathbf{x})\|^2}, \qquad (6.10)$$

where $(\cdot,\cdot)$ and $\|\cdot\|$ are the usual inner product and the norm in $L^2((0,L)^2)$, respectively. In the primitive variables (i.e., before diffusive scaling, which corresponds to taking $\eta = 1$), we recast the fluctuation variations as $|\phi| = 1 + \psi$ so that assuming that ψ is small enough (which is necessary to be in the diffusive regime), we can use the approximation $1 - |\phi|^2 \approx -2\psi$. This implies that the numerical simulations give us access using (4.14) to the quantity

$$F(\psi, |\boldsymbol{\tau}|, |\mathbf{k}|, T, L, k_{\max}, \kappa) = \bar{a}\, J_0(|\boldsymbol{\tau}||\mathbf{k}|)\, \cos(2\psi\Pi_0 T)\, e^{-\frac{\Sigma}{2}\psi^2 T}. \qquad (6.11)$$

The above filter obviously also depends on the choice of the power spectrum $\hat{R}(\mathbf{p})$. To simplify the analysis we choose power spectra that are equal to κ^2 for $|\mathbf{p}| < k_{\max}$ and equal to 0 for $|\mathbf{p}| > k_{\max}$. We thus have a seven parameter family of filters $F(\psi, \boldsymbol{\tau}, |\mathbf{k}|, T, L, k_{\max}, \kappa)$. We recall the meaning of the parameters: ψ measures the change of the fluctuation amplitude of the forward and backward media; $\boldsymbol{\tau}$ represent a shift by $\boldsymbol{\tau}$ between the forward and backward media. Equivalently, it can be seen as a shift by $-\boldsymbol{\tau}$ of the detector array; $|\mathbf{k}|$ is the wavenumber of the source term; T is the propagation time before time reversion; L is the size of the periodic spatial box; $k_{\max}$ measures the support of the power spectrum $\hat{R}(\mathbf{p})$ and κ^2 its intensity. The equation for F also involves two constants, Π_0 and Σ, which are defined in (6.3) and (6.2), respectively.

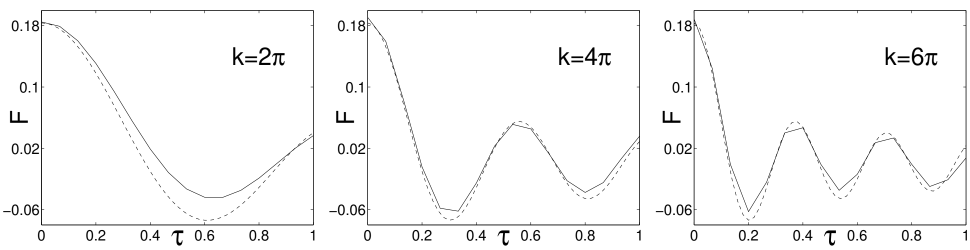

FIG. 6.1. *Numerical simulations of the filter F_{data} (solid lines) and comparison with the theoretical prediction F (dashed lines) for different values of τ with $\psi = 0$. The three columns correspond to initial wavenumbers of $|\mathbf{k}| = 2\pi$, $|\mathbf{k}| = 4\pi$, and $|\mathbf{k}| = 6\pi$, respectively. In all the simulations, the box size is $L = 20$, the propagation time is $T = 200$, the number of modes is 50 so that $k_{\max} = 50\times 2\pi/L$, and the intensity of the fluctuations is $\kappa = L \times 10^{-3}$.*

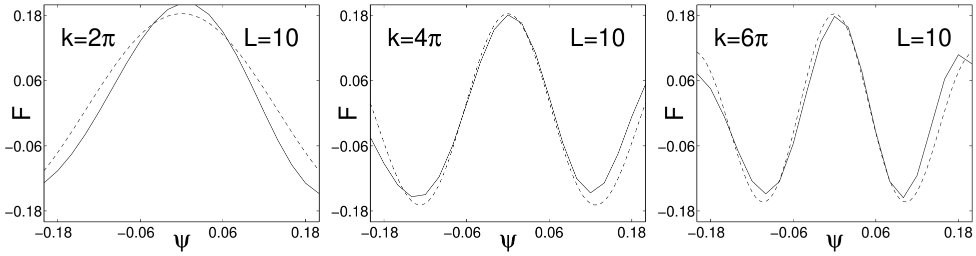

FIG. 6.2. *Numerical simulations of the filter F_{data} (solid lines) and comparison with the theoretical prediction F (dashed lines) for different values of ψ with $\tau = 0$. The three columns correspond to initial wavenumbers of $|\mathbf{k}| = 2\pi$, $|\mathbf{k}| = 4\pi$, and $|\mathbf{k}| = 6\pi$, respectively. In all the simulations, the box size is $L = 10$, the propagation time is $T = 200$, the number of modes is 50 so that $k_{\max} = 50\times 2\pi/L$, and the intensity of the fluctuations is $\kappa = L \times 10^{-3}$.*

Fig. 6.1 shows the behavior of the filter $F(0, |\boldsymbol{\tau}|, |\mathbf{k}|, 200, L, 50 \times 2\pi/L, L \times 10^{-3})$ and of the corresponding F_{data} for $L = 20$ and $|\mathbf{k}| = 2\pi, 4\pi, 6\pi$. We observe the Bessel-type behavior caused by the drift $\boldsymbol{\tau}$ and the linear increase in the oscillation frequency as $|\mathbf{k}|$ grows. In Fig. 6.2, we show for the box $L = 10$ the behavior of the filter $F(\psi, 0, |\mathbf{k}|, 200, L, 50 \times 2\pi/L, L \times 10^{-3})$ and of the corresponding F_{data} for $|\mathbf{k}| = 2\pi, 4\pi, 6\pi$ and for different values of $|\boldsymbol{\tau}|$ with $\psi = 0$ and different values of ψ at $|\boldsymbol{\tau}| = 0$. Fig. 6.3 shows the same results for $L = 20$. The damped oscillatory behavior caused by $\psi \neq 0$ is very well reproduced numerically. Fig. 6.4 shows the

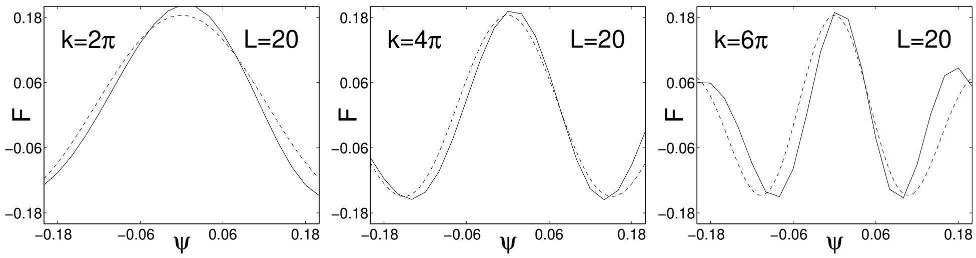

FIG. 6.3. *Same as in Fig. 6.2 with $L = 20$.*

behavior of $\psi \to F(\psi)$ for the same parameters as in Fig. 6.3, second column($L = 20$ and $|\mathbf{k}| = 4\pi$) except that: $T = 400$ so that the frequency of oscillations of $F(\psi)$ is doubled in the first column; $\kappa = L \times 10^{-3}/\sqrt{2}$ so that the frequency is halved in the second column; $M = 25$ in the third column. The latter example shows that the frequency of oscillation of $F(\psi)$ depends very much on the power spectrum $\hat{R}(\mathbf{k})$.

6.5. Reconstructions. The measurement of the experimental filter and the theoretical formula (6.11) can also be used to infer some properties of the medium. One parameter we can consider is the drifting term $|\boldsymbol{\tau}|$. Since the Bessel function is not monotonic, we have to assume something about the drift term, for instance that $|\boldsymbol{\tau}||\mathbf{k}|$ is between the first and the second points at which J_0', the derivative of J_0, vanishes. Assuming that $\bar{a}$ is known and that $\psi = 0$, we observe from the graphs in Fig. 6.1 that $|\boldsymbol{\tau}|$ can be estimated very accurately (less than a few percents) provided that $J_0'(|\boldsymbol{\tau}||\mathbf{k}|)$ is not too close to 0.

Two other parameters we can consider are $\Sigma(\mathbf{k})$ and $\Pi_0(\mathbf{k})$. These parameters can theoretically be reconstructed from $\psi \to F(\psi)$. This implies in practice that

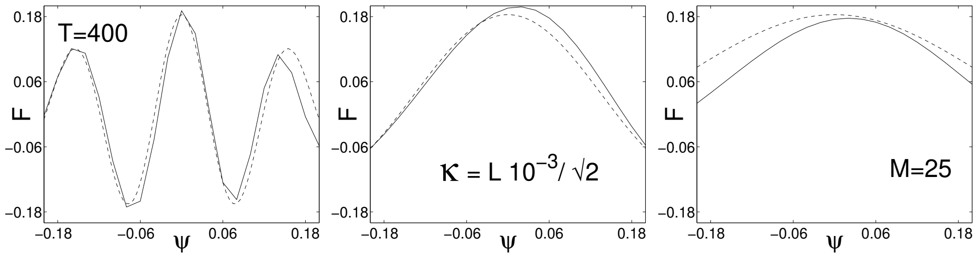

FIG. 6.4. *Numerical simulations of $|\boldsymbol{\tau}| \to F(|\boldsymbol{\tau})$ with $L = 20$ and $k = 4\pi$. The parameters are the same as in the simulation in Fig. 6.3 except that $T = 400$ in the first column, $\kappa = L \times 10^{-3}/\sqrt{2}$ in the second column, and $M = 25$ in the third column. Solid lines are numerical simulations and dashed lines theoretical predictions.*

we control by how much the medium is changed between the forward and backward propagations but do not know the intensity of the fluctuations. In the regime of validity of diffusion, ψ need be sufficiently small. It is therefore very difficult to reconstruct the total scattering coefficient Σ from (6.11). We have observed a very high variability in the reconstruction of the value of Σ that best fits the measured data (on the order of 50% variability depending on the physical parameters and on the realization). The reconstruction of the frequency modulation $\Pi_0(\mathbf{k})$ is much more stable. In our reconstruction, we best fit Π_0 and Σ in $F(\psi)$ given in (6.11) to the numerical data $F_{\rm data}(\psi_i)$ for 21 values of ψ_i uniformly distributed between -0.2 and 0.2. As we have already mentioned, the reconstruction of Σ is not stable. However it does not affect the reconstruction of Π_0 significantly. We present some reconstructions of $\Pi_0(\mathbf{k})$ in Tab. 6.1.

Case		Theory	Reconstruction	Error(%)
Fig. 6.2 column 2	$\lvert\mathbf{k}\rvert = 4\pi$, $L = 10$	$6.05\,10^{-2}$	$5.94\,10^{-2}$	1.8%
Fig. 6.2 column 3	$\lvert\mathbf{k}\rvert = 6\pi$, $L = 10$	$7.41\,10^{-2}$	$7.74\,10^{-2}$	4.3%
Fig. 6.3 column 2	$\lvert\mathbf{k}\rvert = 4\pi$, $L = 20$	$4.97\,10^{-2}$	$5.49\,10^{-2}$	9.5%
Fig. 6.3 column 3	$\lvert\mathbf{k}\rvert = 6\pi$, $L = 20$	$7.02\,10^{-2}$	$8.24\,10^{-2}$	14.8%
Fig. 6.4 column 1	$\lvert\mathbf{k}\rvert = 4\pi$, $T = 400$	$4.97\,10^{-2}$	$5.20\,10^{-2}$	4.3%
Fig. 6.4 column 2	$\lvert\mathbf{k}\rvert = 4\pi$, $\kappa/\sqrt{2}$	$2.49\,10^{-2}$	$2.39\,10^{-2}$	3.8%
Fig. 6.4 column 3	$\lvert\mathbf{k}\rvert = 4\pi$, $M = 25$	$1.23\,10^{-2}$	$1.69\,10^{-2}$	27.3%

TABLE 6.1
Reconstruction of $\Pi_0(\mathbf{k})$ from the measured values $F_{\rm data}(\psi_i)$.

The reconstructions with $|\mathbf{k}| = 4\pi$ are quite good. The reconstruction with $|\mathbf{k}| = 6\pi$ and $L = 20$ (which corresponds to less that 7 grid points per wavelength) becomes less accurate we believe because of numerical effects. In the case of $M = 25$ modes (Fig. 6.4 column 3) the correlation length of the fluctuations becomes large compared to the wavelength. We expect that the radiative transfer regime be less accurate. This is confirmed by the numerical simulation. That reconstructions of $\Pi_0(\mathbf{k})$ are possible with reasonable accuracy shows the quite good agreement between the numerical simulations F_{data} in (6.10) and the theoretical predictions F in (6.11).

6.6. Remarks on the numerical simulations. All the numerical simulations correspond to one single realization of the random medium (we have not averaged over several realizations). It is known that time reversed waves enjoy strong statistical stability [4, 5, 12, 26]. However this may not always be the case [2] as is shown for time reversal in changing one-dimensional media [1]. The numerical simulations seem to suggest that with the environment changes considered here with $\phi(\mathbf{x},\mathbf{k})$ deterministic, the time reversed waves are indeed statistically stable.

The radiative transfer equations are different in the whole medium $\mathbb{R}^2$ and in the periodic box L^2 where wavenumbers are quantized. Only in the limit $L \to \infty$ do the models agree. We have observed that the numerical simulations were already quite satisfactory with $L = 10$ (with a sound speed $c_0 = 1$). Results with $L = 20$ were also satisfactory for $|\mathbf{k}| \leq 6\pi$. For $|\mathbf{k}| = 8\pi$, $L = 20$, and $N_x = 400$, there are only 5 discretization points per wavelength and we have observed much larger discrepancies between numerics and theory. Values of $L = 10, 20$ are therefore a good compromise between accuracy of the model on a periodic box and requirements on the number of discretization points per wavelength.

7. Conclusions. We have considered the refocusing properties of time-reversed waves that propagate in different media during the forward and backward stages. We have used generalizations of the radiative transfer and diffusive regimes to characterize the refocusing when the fluctuations of the backward and forward propagation media are related by $\hat{\kappa}_2(\mathbf{x},\mathbf{k}) = \phi(\mathbf{x},\mathbf{k})\hat{\kappa}_1(\mathbf{x},\mathbf{k})$ with $\phi(\mathbf{x},\mathbf{k})$ a deterministic function. The effects of simple environment changes such as $\phi \in \mathbb{R}$ and $\phi = e^{i\boldsymbol{\tau}\cdot\mathbf{k}}$ have been emphasized in the diffusive regime, where the mathematical description for the refocusing is relatively compact. We have underlined several oscillatory behaviors of the refocusing as media changes occur: multiplication by a sinc function (a Bessel function in two space dimensions) when the medium is shifted, and multiplication by a time-dependent oscillatory term and a damping factor when the changes in the medium are such that scattering is no longer elastic. We have obtained a very good agreement between numerical simulations and theoretical predictions for these behaviors.

Acknowledgment. This work was supported by ONR Grant N00014-02-1-0089. GB was supported in part by NSF Grant DMS-0239097 and an Alfred P. Sloan fellowship.

REFERENCES

[1] D. G. Alfaro Vigo, J.-P. Fouque, J. Garnier, and A. Nachbin, *Robustness of time reversal for waves in time-dependent random media*, Submitted, (2003).
[2] G. Bal, *On the self-averaging of wave energy in random media*, Submitted, (2003).
[3] G. Bal, V. Freilikher, G. Papanicolaou, and L. Ryzhik, *Wave Transport along Surfaces with Random Impedance*, Phys. Rev. B, 62(10) (2000), pp. 6228–6240.
[4] G. Bal, T. Komorowski, and L. Ryzhik, *The Liouville transport equation for classical waves in random media*, to appear in Comm. Math. Phys., (2003).
[5] G. Bal, G. Papanicolaou, and L. Ryzhik, *Self-averaging in time reversal for the parabolic wave equation*, Stochastics and Dynamics, 4 (2002), pp. 507–531.
[6] G. Bal and L. Ryzhik, *Time Reversal and Refocusing in Random Media*, SIAM J. Appl. Math., 63(5) (2003), pp. 1475–1498.
[7] ———, *Time splitting for wave equations in random media*, Submitted, (2003).
[8] C. Bardos and M. Fink, *Mathematical foundations of the time reversal mirror*, Asymptotic Analysis, 29(2) (2002), pp. 157–182.
[9] J. Berryman, L. Borcea, G. Papanicolaou, and C. Tsogka, *Statistically stable ultrasonic imaging in random media*, J. Acoust. Soc. Amer., 112 (2002), pp. 1509–1522.
[10] P. Blomgren, G. Papanicolaou, and H. Zhao, *Super-Resolution in Time-Reversal Acoustics*, J. Acoust. Soc. Am., 111(1) (2002), pp. 230–248.
[11] B. Borcea, C. Tsogka, G. Papanicolaou, and J. Berryman, *Imaging and time reversal in random media*, Inverse Problems, 18 (2002), pp. 1247–1279.

[12] J. F. Clouet and J.-P. Fouque, *A time-reversal method for an acoustical pulse propagating in randomly layered media*, Wave Motion, 25 (1997), pp. 361–368.

[13] R. Dautray and J.-L. Lions, *Mathematical Analysis and Numerical Methods for Science and Technology. Vol.6*, Springer Verlag, Berlin, 1993.

[14] A. Derode, A. Tourin, J. de Rosny, M. Tanter, S. Yon, and M. Fink, *Taking advantage of multiple scattering to communicate with time reversal antennas*, Phys. Rev. Lett., 90 (2003), p. 014301.

[15] G. F. Edelmann, T. Akal, W. S. Hodgkiss, S. Kim, W. A. Kuperman, and H. C. Song, *An Initial Demonstration of Underwater Acoustic Communication Using Time Reversal*, IEEE J. Oceanic Eng., 27 (2002), pp. 602–609.

[16] L. Erdös and H. T. Yau, *Linear Boltzmann equation as the weak coupling limit of a random Schrödinger Equation*, Comm. Pure Appl. Math., 53(6) (2000), pp. 667–735.

[17] M. Fink, *Time reversed acoustics*, Physics Today, 50(3) (1997), pp. 34–40.

[18] ———, *Chaos and time-reversed acoustics*, Physica Scripta, 90 (2001), pp. 268–277.

[19] M. Fink, G. Montaldo, and M. Tanter, *Time reversal acoustics in biomedical engineering*, Ann. Rev. Biomed. Eng., 5 (2003), pp. 465–497.

[20] M. Fink and C. Prada, *Acoustic time-reversal mirrors*, Inverse Problems, 17(1) (2001), pp. R1–R38.

[21] J.-P. Fouque and K. Sølna, *Time-reversal aperture enhancement*, SIAM Mult. Mod. Simul., 1 (2003), pp. 239–259.

[22] W. Hodgkiss, H. Song, W. Kuperman, T. Akal, C. Ferla, and D. Jackson, *A long-range and variable focus phase-conjugation experiment in shallow water*, J. Acoust. Soc. Am., 105 (1999), pp. 1597–1604.

[23] W. Kuperman, W. Hodgkiss, H. Song, T. Akal, C. Ferla, and D. Jackson, *Phase-conjugation in the ocean*, J. Acoust. Soc. Am., 102 (1997), pp. 1–16.

[24] E. W. Larsen and J. B. Keller, *Asymptotic solution of neutron transport problems for small mean free paths*, J. Math. Phys., 15 (1974), pp. 75–81.

[25] G. Papanicolaou, L. Ryzhik, and K. Sølna, *The parabolic approximation and time reversal*, Matem. Contemp., 23 (2002), pp. 139–159.

[26] ———, *Self-averaging of Wigner transforms in random media*, to appear in SIAM J. App. Math., (2003).

[27] L. Ryzhik, G. Papanicolaou, and J. B. Keller, *Transport equations for elastic and other waves in random media*, Wave Motion, 24 (1996), pp. 327–370.

[28] P. Sheng, *Introduction to Wave Scattering, Localization and Mesoscopic Phenomena*, Academic Press, New York, 1995.

[29] A. Tourin, A. Derode, and M. Fink, *Sensitivity to perturbations of a time-reversed acoustic wave in a multiple scattering medium*, Phys. Rev. Lett., 87 (2001), p. 274301.